

Asymmetry in Isolated, Morphologically Normal Sa Galaxies

David A. Kornreich¹

Center for Radiophysics and Space Research
Cornell University Space Sciences Building, Ithaca NY 14853
kornreic@astro.cornell.edu

Martha P. Haynes

Center for Radiophysics and Space Research and National Astronomy and Ionosphere Center²
Cornell University Space Sciences Building, Ithaca NY 14853
haynes@astro.cornell.edu

Katherine P. Jore

Department of Physics and Astronomy, University of Wisconsin at Stevens Point, Stevens Point WI 54481
kjore@uwsp.edu

and

R. V. E. Lovelace

Department of Astronomy
Cornell University Space Sciences Building, Ithaca NY 14853
rvl1@cornell.edu

ABSTRACT

We have examined the morphological and dynamical H I symmetry properties of a sample of moderately inclined Sa galaxies which are classified as morphologically normal. The sample galaxies were known *a priori* to exhibit kinematic peculiarities ranging from warps to independent, wholly decoupled disks, and are possibly the remnants of minor mergers. We compare the asymmetry of the rotation curves to global kinematic asymmetry, and find a relationship between rotation curve asymmetry and the kinematic $n = 2$ mode. We have also examined the kinematics of these galaxies following the discussion of Briggs (1990) and find that the warps observed in the H I disks of these galaxies deviate significantly from the simple rules for warps that commonly apply.

Subject headings: galaxies: kinematics and dynamics — galaxies: structure

1. Introduction

Minor mergers are a prime candidate for the excitation of asymmetries in galaxies, both kinematic and morphological. As such, it is important to investigate the symmetry properties of galaxies believed to be the remnants of minor mergers when seeking to understand the nature of the resulting perturbations.

¹NASA Space Grant Graduate Fellow

²The National Astronomy and Ionosphere Center is operated by Cornell University under a cooperative agreement with the National Science Foundation.

As part of a study to investigate the homogeneity and dark matter content of the Sa galaxy class, Jore (1997) investigated the dynamics of gas and stars in a sample of 20 nearby, morphologically normal, isolated Sa galaxies. For nine gas-rich objects, H I synthesis maps were obtained with the Very Large Array (VLA)³.

Although Jore’s sample was selected to be isolated and morphologically normal, several cases of peculiar kinematics were discovered. Jore *et al.* (1996; hereafter Paper I) discussed NGC 4138, an isolated Sa containing coplanar counter-rotating stellar disks embedded in an extensive H I disk. Haynes *et al.* (2000; hereafter Paper II) discuss optical photometry and spectroscopy obtained for four galaxies: NGC 3626, NGC 3900, NGC 4772, and NGC 5854, and H I synthesis line imaging for the first three of these, all of which exhibit some form of counter-rotation or kinematically distinct ionized gas components. Jore *et al.* (2000; hereafter Paper III) discuss optical and H I synthesis data obtained for the remaining VLA targets: NGC 1169, NGC 3623, NGC 4866, NGC 5377, and NGC 5448. Of these galaxies, too, three (NGC 3623, NGC 4866, and NGC 5377) exhibit indications of kinematic decoupling in their optical spectra. NGC 5448, although kinematically regular as traced optically, exhibits an inner disk that is non-coplanar with the outer disk as defined beyond half the optical radius, $0.5R_{25}$.

The galaxies studied in Papers I–III contain moderate H I masses spread over a large area, with $R_{HI}/R_{25} > 2$, so that the neutral gas surface density is very low. The only exception, NGC 3623, is gas poor with a shrunken H I disk. It also is the only galaxy with nearby major companions, and is in fact a member of the Leo Triplet (Haynes *et al.* 1979).

The details of the observations and data analysis leading to the conclusions of kinematic decoupling in these galaxies is discussed exclusively in Papers I–III. In this work, we offer no further evidence for their existence. Here, instead, our intent is not to produce detailed kinematic models of these targets, but rather to classify the kinematic and morphological asymmetry exhibited by the H I disks and to compare their global H I rotation curve properties to sets known to be dynamically normal, and thus to demonstrate that decoupled components as observed in optical spectra occur in galaxies with abnormal warps and global rotation curves in the H I.

The most commonly accepted explanation of the occurrence of kinematically distinct components is that of minor mergers (see, for example, Thakar *et al.* 1997), which have been proposed to account for the counter-rotating disks of NGC 7217 (Merrifield & Kujiken 1994; Buta *et al.* 1995), NGC 3593 (Bertola *et al.* 1996; Corsini *et al.* 1998), NGC 3626 (Ciri *et al.* 1995), and NGC 4138 (Paper I). Thakar *et al.* have been able to produce by numerical simulation morphologically symmetric counter-rotating disks via both gradual infall and minor mergers. The main drawback is that minor mergers tend to heat the disk significantly. Conversely, Zaritsky & Rix (1997) observe morphological lopsidedness and interpret their derived statistic that 30% of field disks are asymmetric as evidence of ongoing mass infall at a rate of about 2% of the disk mass per Gyr. Quinn *et al.* (1993) have also numerically studied the effects of minor mergers, and predict that mergers with satellite galaxies generally result in a heating of the entire disk around all three axes, as well as the generation of a long-lived warp in disk inclination of order 15° . The numerical work of Hernquist & Mihos (1995) studied similar mergers and characterized their dynamics, finding significant excitation of $n = 2$ spiral modes at a level of approximately 20% of the total observed power in all Fourier components and of the $n = 1$ and $n = 3$ modes at lesser levels.

³The VLA is a part of the National Radio Astronomy Observatory, which is a facility of the National Science Foundation operated under a cooperative agreement by Associated Universities, Inc.

The deviations from morphological and kinematic axisymmetry can be quantified in a number of ways. Zaritsky & Rix quantify morphological asymmetry by dividing the galaxy into a set of concentric rings and then measuring the Fourier strengths of the flux through each ring. This method has the advantage of identifying the type and strength of the asymmetry as a function of radius, but cannot be used with small, distant objects due to data scarcity. More widely applicable methods are those which consider the galaxy as a whole; such methods miss any radial dependence, but do not suffer as strongly in small data sets (because they integrate large portions of the image) and are quick and dirty ways of identifying nonaxisymmetries. Conselice (1997), for instance, suggests rotating a galaxy image through 180° (or some other convenient angle) and subtracting the resultant image from the original. The residuals are taken as the asymmetry measure. Kornreich *et al.* (1998; hereafter KHL) propose dividing the galaxy into a number (usually 8) of sectors centered on the optical center of light of the galaxy and integrating the flux in each sector. The greatest normalized difference between sectors is taken as the asymmetry measure.

Deviations from flat, circular motion in galaxies have been quantified in H I synthesis data by Kornreich *et al.* (2000; hereafter KHLvZ). Since flat, circular motion implies a constant kinematic position angle as a function of radius, kinematic asymmetry has been quantified as average changes in position angle, either as a function of radius or between approaching and receding sides in model velocity fields. Kinematic nonaxisymmetry can also manifest as differences in the rotation curves of the approaching and receding sides, and the normalized integrated rotation curve differences are also taken as quantifiers of non-axisymmetry (Schoenmakers *et al.* 1997, hereafter SFdZ).

Here our goal is to identify and quantify the axisymmetry of the dynamics of the nine H I-rich galaxies in the sample of Jore (1997) mapped with the VLA in terms of the asymmetry parameters of KHLvZ. The more inclined aspect at which these galaxies are viewed, with respect to the sample of KHLvZ, allows the dynamical parameters to be determined with much greater precision. We will also compare the dynamics of this sample with that of the sample of Briggs (1990), a sample of warped but otherwise kinematically normal galaxies, to determine whether the kinematically peculiar sample follows the same pattern of warps detected there.

2. The Sa Galaxy Sample

The nine objects selected for this analysis are a subset of the sample of isolated, morphologically normal Sa galaxies originally selected by Jore (1997) in her study of Sa kinematics and dynamics. The subset discussed here and summarized in Table 1 were selected because they are relatively HI-rich, making H I synthesis observations with the VLA feasible. The columns of Table 1 represent:

- (1) The NGC designation of the target galaxy;
- (2) The morphological classification as given in the *Revised Shapley Ames Catalog* (Sandage & Tammann 1987).
- (3) The optical major and minor diameters at 25 mag arcsec⁻², taken from the *Third Reference Catalog of Bright Galaxies* (de Vaucouleurs *et al.* 1991; RC3).
- (4) Type of distinct kinematics detected in the optical spectroscopy by Papers I–III, except for NGC 1169 and NGC 5448, where the kinematic peculiarity is seen only in the H I disk; and
- (5) Reference for the data presentation and discussion.

For each object, an R -band image was obtained with the Kitt Peak⁴ 0.9 meter telescope and a 21 cm H I line synthesis map was made with the VLA in either the C or D configuration. For details of the datasets and their acquisition and reduction procedures, see Papers I–III and §3.3.2 of Jore (1997). Here we discuss only those aspects that are specific to the current work.

3. Data Analysis

3.1. Obtaining Derived Rotation Curves

The moment maps representing the H I velocity fields obtained from Papers I–III were analyzed in the GIPSY environment (van der Hulst *et al.* 1992, *GIPSY* 2000). Rotation curves were derived by iteratively applying the standard GIPSY routine ROTCUR (Begeman 1989). This routine divides the galaxy into a number of rings, and fits a function

$$V(x, y) = V_{sys} + V_{rot} \cos \theta \sin i \quad (1)$$

where

$$\cos \theta = \frac{-(x - x_0) \sin(\Gamma) + (y - y_0) \cos(\Gamma)}{r} \quad (2)$$

to the velocity field in each ring, allowing the systematic velocity V_{sys} , the rotation velocity V_{rot} , inclination i , position angle Γ , and kinematic center (x_0, y_0) to vary. The implicit assumption is that the gas falls in nearly flat, circular orbits. The normal morphology of the galaxies studied here suggests that this is likely the case.

Because the H I in NGC 3626 is made up of independent inner and outer rings (see Paper II), these rings were fit independently of one another, and later combined into a single model.

The tilted-ring model fits were obtained iteratively in the following way. The velocity fields of each galaxy were fit, using a $\cos \theta$ weighting function, and allowing all parameters to vary. The purpose of this first fit was to find the kinematic center or centers of the galaxy. In some cases, the kinematic center differed by more than a beam width between the inner and outer regions of the disk. In these cases, two independent centers, c_1 and c_2 were fit to the inner and outer regions, respectively. The derived kinematic centers are presented in Table 2.

The columns represent the galaxy designation, the right ascension and declination of the derived kinematic center c_1 (or kinematic center of the inner disk, where two centers were fit), the kinematic center of the outer disk c_2 , where two centers were fit, and the boundary radius R_b between the inner and outer fits. In all cases, the derived (inner) center c_1 agrees with the kinematic centers derived in Papers I–III using a slightly different approach.

Following the fit of the kinematic centers, the approaching and receding sides of the galaxy were fit separately, with the kinematic centers fixed. In cases where two centers were derived, inner ($r \leq R_b$) and outer ($R > R_b$) regions were fit independently. The fit obtained for both sides used as the initial guess in the iteration. The results of these fits then represented the rotation velocity V_{rot} , the inclination i , and the

⁴The Kitt Peak National Observatory is a facility of the National Optical Astronomy Observatories, which is operated by the Association of Universities for Research in Astronomy, Inc. (AURA) under a cooperative agreement with the National Science Foundation.

Table 1. Overview of the Sa Sample

Galaxy	Type	$D_{25} \times d_{25}$ (arcmin)	Peculiar Optical Kinematics (except where otherwise noted)	Ref.
NGC 1169	SB(r)a I	4.17×2.82	Strong H I warping	a
NGC 3623	S(s)a II	9.77×2.88	Counter-Rotating Gas Core	a
NGC 3626	Sa	2.69×1.95	Extended Counter-Rotating Gas	b
NGC 3900	S(r)a	3.16×1.70	Central High-Velocity Gas? Streaming?	b
NGC 4138	S(r)a pec	2.57×1.70	Extended Counter-Rotating Gas, Stars	c
NGC 4772	Sa:	3.39×1.70	Counter-Rotating Gas Core	b
NGC 4866	Sa	6.31×1.35	Nonrotating Gas	a
NGC 5377	SBa	3.72×2.09	Counter-Rotating Gas?	a
NGC 5448	S(s)a	3.98×1.78	Twisting of Inner H I Position Angles	a

^aJore *et al.* (2000)

^bHaynes *et al.* (2000)

^cJore *et al.* (1996)

Table 2. Derived Kinematic Centers

Galaxy	c_1 (1950)		c_2 (1950)		R_b (arcsec)
	α	δ	α	δ	
NGC 1169	030011.1	+461129.3	030011.9	+461140.0	240
NGC 3623	111619.2	+132157.9
NGC 3626	111726.2	+183746.4	111725.9	+183752.6	52
NGC 3900	114633.8	+271759.9
NGC 4138	120658.1	+435748.9	120659.4	+435730.9	140
NGC 4772	125056.2	+022614.9
NGC 4866	125658.3	+142623.9
NGC 5377	135417.8	+472845.7
NGC 5448	140055.9	+492443.3

position angle Γ as a function of radius. These fits are presented in Figure 1. For each galaxy frame, the radius is given on the x axis in arcseconds, while V_{rot} , i , and Γ are given on the y axis in km s^{-1} , degrees, and degrees, respectively. Circles and solid lines trace the approaching side, while triangles and dotted lines trace the receding side.

3.2. Construction of Tip–LON Diagrams

Briggs (1990) has employed a graphical representation of position angle versus inclination as functions of radius to illustrate the degree and character of warping in H I disks. Because the tilted–ring fits in this work were accomplished with independent V_{rot} and i , it was possible to represent the changes in the dynamic structure of the galaxies via these position–angle/inclination diagrams. These “tip–LON” diagrams are useful for studying the structure of galactic warping and kinematic bending of the disk. The plots represent the kinematic orientation (or “tip angle”) of the rings, as a function of radius, referred back to the average plane of the galaxy.

All of the information of the position angle Γ and inclination i at radius R is contained within the vector normal to the plane of the fitted ring. If we define a hemisphere with the galaxy at the center of the circular base, and where the base represents the plane of the sky as seen from Earth, such that the telescope lies directly above the apex of the hemisphere, then the set of points of intersection of the hemisphere with the normal vectors will also contain all of the information contained within Γ and i . The resulting points are located at a “latitude” equal to $90^\circ - i$, and “longitude” $\Gamma + 90^\circ$ (See Figure 1 of Briggs 1990). The azimuthal coordinate corresponds to the direction 90° from the line of nodes (LON) of the ring in the reference plane, hence the name “tip–LON” diagram adopted by Briggs.

Once the points on the hemispherical surface are determined, the points are then projected onto a plane, tangent to the sphere at the point representing the first ring, or at some other convenient nearby point. The final result is a spherical projection mapping the kinematic orientation for all radii. For a more detailed description of the mapping procedure, see Briggs (1990).

The tip–LON diagrams for the current inclined Sa galaxy sample are presented in Figure 2. In these diagrams, as in the rotation curves, circles and solid lines represent the approaching side of the galaxy; triangles and dashed lines the receding side. Also included in each diagram is a single point, represented as an open star, indicating the observed morphological tip angle of the optical galaxy as determined by isophotal ellipse fitting of the isophote at R_{25} in the R –band images from Papers I–III as performed using the GALPHOT⁵ package of IRAF⁶/STSDAS⁷. The solid line radiating from the center of the plot indicates the direction away from the line of sight, such that deviations roughly parallel to this line represent deviations in i . Deviations perpendicular to this line represent mostly deviations in Γ . The large, concentric, dotted circles each represent 10° deviation (or “tip”) from the tangent point, located at the center of the diagram. Note that each diagram is cut off at a different maximum deviation. For each diagram, the tangent point is chosen to be the first fitted ring point on the approaching side, except where this point is

⁵The GALPHOT surface photometry package is a collection of IRAF/STSDAS scripts originally developed by Wolfram Freudling and John Salzer; the Cornell version has been further modified and is maintained by M. P. H.

⁶IRAF is distributed by the National Optical Astronomy Observatory.

⁷STSDAS (Space Telescope Science Data Analysis System) is distributed by the Space Telescope Science Institute which is operated by AURA under contract to the National Aeronautics and Space Administration.

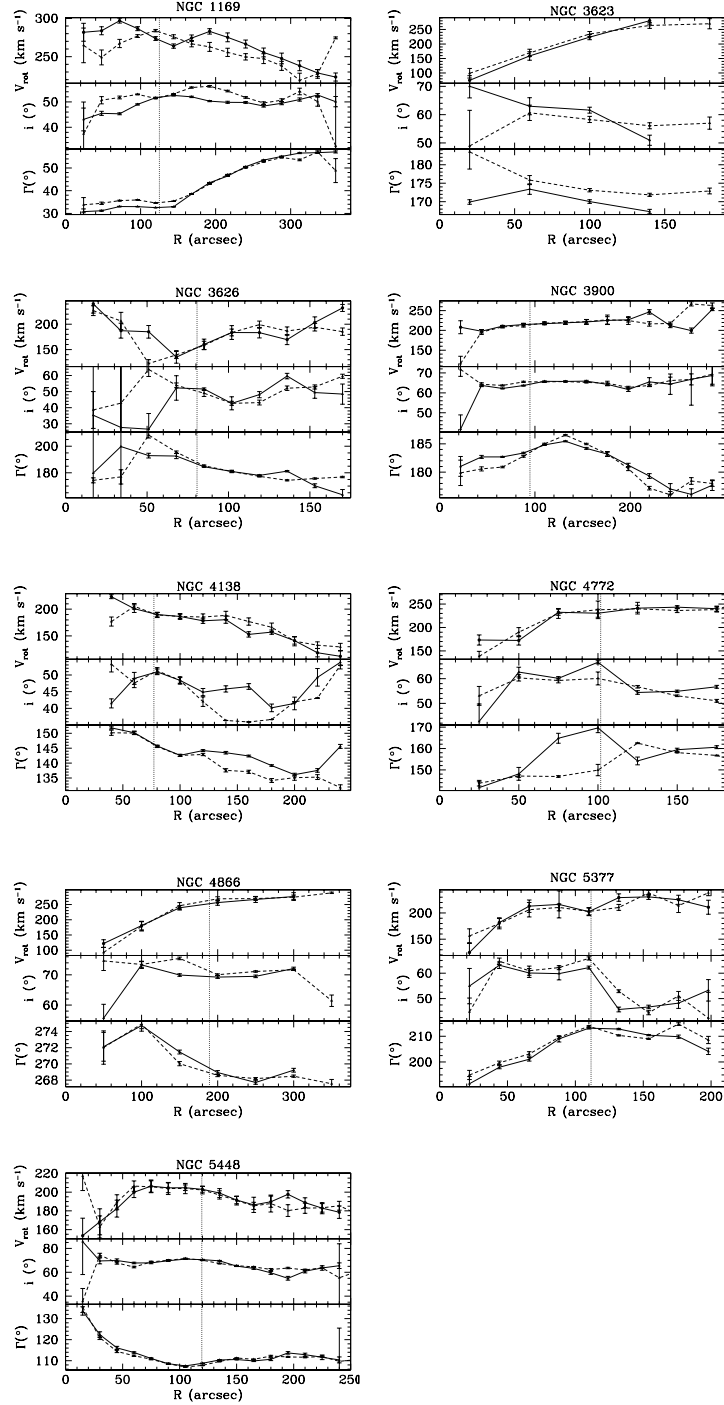


Fig. 1.— Rotation curves and position angle plots derived from the tilted-ring fitting for the nine galaxies in the Sa sample. The x axis of each frame is the radius of the galaxy in arcseconds, while the y axes of each frame, are, top to bottom, the derived rotation V_{rot} , the derived kinematic inclination i in degrees, and the derived kinematic position angle Γ , also in degrees. Solid lines represent the fit for the approaching side; dashed lines that of the receding side. The vertical dotted line in each frame represents R_{25} .

of large uncertainty or is isolated from the rest of the plotted points. In those cases, the point of tangency is chosen to be the second plotted point on the approaching side. A disk rotating in a flat plane, free of warps and streaming motions, should have all its points concentrated in the center of the diagram.

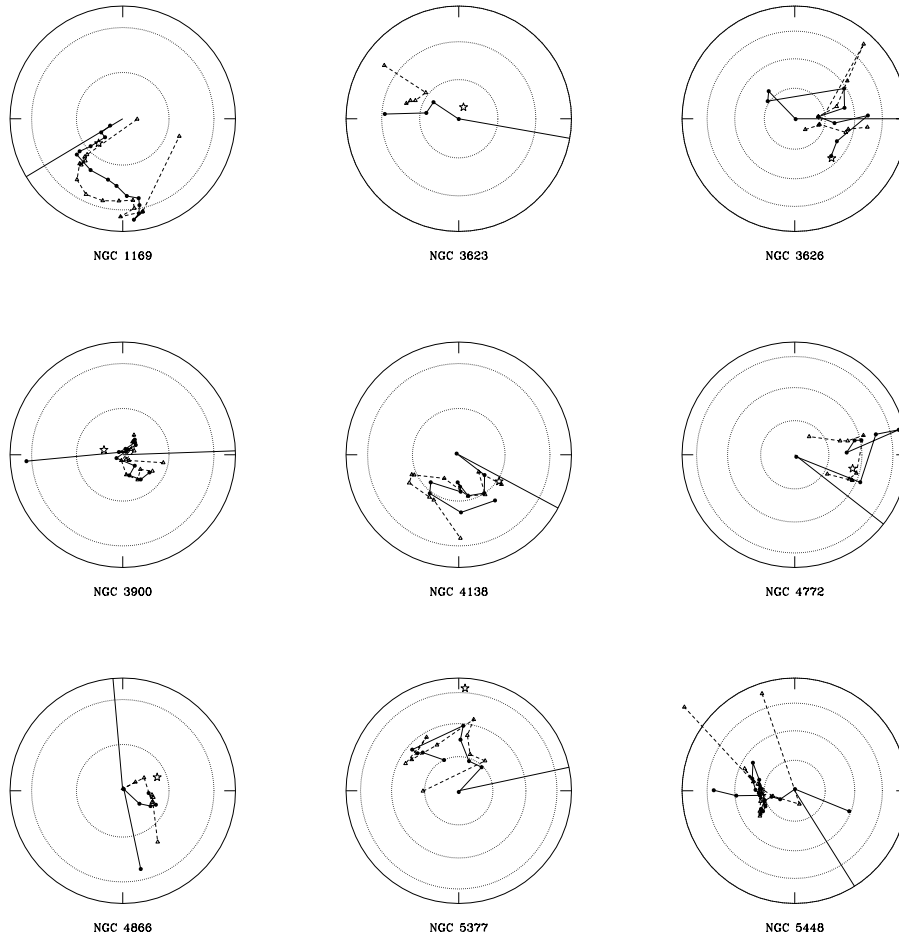


Fig. 2.— Tip-LON diagrams for the nine galaxies in the sample. Both the approaching (circles, solid lines) and receding (triangles, dashed lines) are presented. The open star in each diagram represents the morphological tip angle derived from the R -band optical isophote at D_{25} . The solid line extending from the center of the diagram to the outer circle indicates the direction away from the $i = 0^\circ$ pole, indicating the direction of increasing inclinations. Successive dotted concentric circles are of 10° deviation each.

3.3. Analysis of Nonaxisymmetries

In KHL and KHLvZ, we discussed methods for quantifying the morphological and dynamical asymmetry of a galaxy. Morphological asymmetry can be measured in either the optical or H I regimes using the “Method of Sectors” described in KHL. First, some appropriate center of the galaxy is determined; this center can be the optical center of light, the dynamical center, or some other appropriate choice. Radials

are then drawn outward from the center, dividing the galaxy into a number n (usually 8) of sectors. Inner and outer boundary radii are then selected inside of which flux integration will be performed. Generally, the inner radius is selected to leave out contributions from the bulge or bar components, while the outer radius is selected to include as much flux from the galaxy as possible while minimizing noise. The flux is then integrated inside each sector. The maximum flux difference is then normalized to the total measured flux to produce the asymmetry measure

$$A_f = \frac{f^{max} - f^{min}}{\sum_n f_n}, \quad (3)$$

where f^{max} and f^{min} are the maximum and minimum flux detected in a sector, and f_n is the flux in the n th sector. For galaxies observed at inclinations other than face-on, the sector pattern can be projected to the appropriate angle.

Quantifying dynamical asymmetry was performed in KHLvZ by examining the rotation curves of target galaxies. In a perfectly axisymmetric disk, approaching and receding rotation curves should be identical, and the kinematic position angle should be constant as a function of radius and between the approaching and receding sides. The measure of rotation curve symmetry is performed by superposing the approaching and receding sides of the rotation curve and integrating the differences between them, normalized by half of the velocity width. In KHLvZ, measurements were taken using the observed rotation curves:

$$S_2^{obs} \equiv 10^2 \times \frac{\int ||V_{rot}(r) \sin i| - |V_{rot}(-r) \sin i|| dr}{\int \frac{1}{2} [|V_{rot}(r) \sin i| + |V_{rot}(-r) \sin i|] dr}. \quad (4)$$

To quantify the deviations from constant position angle, two measurements were taken. First, the maximum difference in position angle as a function of radius

$$\Delta\Gamma(r)|_{>} = \max |\Gamma(r_n) - \Gamma(r_m)|, \quad (5)$$

where n and m are indices of rings in the tilted-ring fit on the same side (approaching or receding) of the fit, and second, the average of position angle differences between sides:

$$\Delta\Gamma(\theta) = \frac{1}{n} \sum_n |\Gamma(-r_n) - \Gamma(r_n)|. \quad (6)$$

Note that the latter two parameters are introduced simply as $\Delta\Gamma(r)$ and $\Delta\Gamma(\theta)$ in KHLvZ.

Finally, Haynes *et al.* (1998) describe the measurement of asymmetry in H I line profiles. The quantity defined there is:

$$A_{l/h} \equiv \frac{\int_{V_l}^{V_{med}} S dV}{\int_{V_{med}}^{V_h} S dV} \quad (7)$$

where V_l and V_h are the low and high velocity limits, respectively, of signal detection above 3σ , and V_{med} is the median between them. The characteristic lopsidedness of the line profile is given simply by

$$A_n \equiv \begin{cases} A_{l/h}, & \text{if } A_{l/h} > 1 \\ 1/A_{l/h}, & \text{otherwise.} \end{cases} \quad (8)$$

Following the discussion in KHLvZ, and using the fitted rotation curves, the dynamical parameters of the observed rotation curve asymmetry S_2^{obs} (equation 4), the derived rotation curve asymmetry

$$S_2^{drv} \equiv 10^2 \times \frac{\int ||V_{rot}(r)| - |V_{rot}(-r)|| dr}{\int \frac{1}{2} [|V_{rot}(r)| + |V_{rot}(-r)|] dr}, \quad (9)$$

the maximum change in position angle with radius $\Delta\Gamma(r)|_{>}$, and the average difference in position angle between approaching and receding sides at constant radius $\langle\Delta\Gamma(\theta)\rangle$ were calculated. Here, we expand this analysis to calculate the average difference in position angle with radius on the same side, $\langle\Delta\Gamma(r)\rangle$, and the maximum change in position angle at constant radius between sides, $\Delta\Gamma(\theta)|_{>}$.

The zeroth moment maps representing the H I column density obtained from Papers I—III were also analyzed in the GIPSY environment following the discussion of morphological asymmetry quantification described in KHLvZ, using a total of eight segments each. Because all of the galaxies in this sample are inclined, the segment pattern had to be projected to the position angle and inclination of the target galaxies, averaged over all radii. The segments were numbered 1 through 8, with segment number 1 being located just north of the western semi-major axis, and with the remaining segments numbered consecutively in a counter-clockwise fashion. No corrections were made for internal extinction.

The R -band images were analyzed for morphological asymmetry using the “Method of Sectors” described in KHL. Foreground stars and other interfering objects were removed from the optical frame by replacing them with a second-order polynomial interpolation of the surrounding background before the segment analysis.

Finally, the synthesized H I line profiles obtained from Papers I—III were analyzed for asymmetry following the discussion of Haynes *et al.* (1998).

The results of the asymmetry quantifiers are presented in Table 3. The columns in this table represent:

- (1) The NGC designation of the galaxy;
- (2) The morphological asymmetry $A_{f,R}$ obtained from the segmented flux comparison in the R -band. Following the value of $A_{f,R}$, the maximum and minimum flux segments are identified by number in parentheses;
- (3) The morphological asymmetry $A_{f,HI}$ obtained from the segmented flux comparison in H I. Following the value of $A_{f,HI}$, the maximum and minimum flux segments are identified by number in parentheses;
- (4) The observed rotation curve asymmetry S_2^{obs}
- (5) The derived rotation curve asymmetry S_2^{drv} ;
- (6) The mean difference in position angle with radius on the same side, $\langle\Delta\Gamma(r)\rangle$;
- (7) The mean difference in position angle on opposite sides at the same radius, $\langle\Delta\Gamma(r)\rangle$;
- (8) The greatest difference in position angle with radius on the same side, $\Delta\Gamma(r)|_{>}$;
- (9) The greatest difference in position angle on opposite sides at the same radius, $\Delta\Gamma(r)|_{>}$; and
- (10) The asymmetry in the synthesized H I line profiles, A_n .

4. Discussion

4.1. Asymmetry Characteristics of the Sa Sample

The Jore (1997) sample of Sa galaxies was selected based on normal optical morphology; therefore, it is not surprising to find that the measurements of optical asymmetry for these galaxies are small when

compared to similar measurements of lopsided galaxies in KHLvZ. Only two galaxies in this sample exhibit significant asymmetry ($A_{f,R} > 0.03$) as measured by this method: NGC 3623 and NGC 5377. The asymmetry measurement for NGC 3623 reflects the prominent dust lanes observed in the eastern portions of the galaxy, while that of NGC 5377 reflects the presence of a low–surface–density outer disk at an apparent position angle different from that of the inner disk.

This apparently quiescent story changes when the H I disks are examined. Large values of the H I morphological asymmetry $A_{f,HI}$ and the various $\Delta\Gamma$ parameters are observed throughout the sample. Most values of S_2 detected in this sample do not rise to the amplitude of those detected in KHLvZ, but this may reflect two significant effects: first, the difficulty of obtaining adequate rotation curves for the face–on galaxies of KHLvZ, and second, that large values of S_2 in face–on objects primarily reflect non–planar motions, while in inclined objects they reflect non–circular motions. Therefore, these results indicate that non–circular motions in the Sa sample are of lesser magnitude than the non–planar motions in the face–on sample.

Nevertheless, the asymmetry detected in the rotation curves of these kinematically disturbed galaxies is still of order 4–10%, significantly larger than the 1–2% asymmetry in the $n = 2$ spiral mode measured by SFDz for the kinematically normal galaxies NGC 2403 and NGC 3198.

The dichotomy between the small asymmetries measured in the optical and the large asymmetries measured in the H I is not surprising; it only confirms the reports of kinematic decoupling discussed in Papers I–III. Thus these findings suggest the hypothesis that the stellar component, evident in the optical images, recovers from the disruptive event which caused the kinematic decoupling more quickly than the hydrodynamic components, and that galaxies with disturbed kinematics can still appear morphologically normal.

4.2. Evaluation of Briggs’ Rules for Warps in the Sa Sample

Briggs (1990) has studied the characteristics of warps in a sample of 12 galaxies whose kinematics were determined from H I synthesis maps. From his sample, he inferred four rules of behavior for warps in galactic disks: first, that disks are planar within R_{25} , but warping in inclination becomes evident at the Holmberg radius $R_{Ho} \equiv R_{26.5}$. Second, that warps change character at a transition radius near R_{Ho} . Third,

Table 3. Asymmetry Measures of the Sa Sample

Galaxy	$A_{f,R}$	$A_{f,HI}$	S_2^{obs}	S_2^{drv}	$\langle\Delta\Gamma(r)\rangle$ ($^\circ$)	$\langle\Delta\Gamma(\theta)\rangle$ ($^\circ$)	$\Delta\Gamma(r) _>$ ($^\circ$)	$\Delta\Gamma(\theta) _>$ ($^\circ$)	A_n
NGC 1169	0.0248 (4,8)	0.0534 (6,3)	1.20	2.87	1.8 ± 0.12	2.25 ± 1.7	26.3 ± 1.3	9 ± 0.3	1.01
NGC 3623	0.0441 (3,6)	0.1110 (3,1)	2.42	7.32	-1.9 ± 1.0	13.5 ± 4.7	11.6 ± 4.6	5.9 ± 2.0	1.11
NGC 3626	0.0208 (2,4)	0.1086 (5,3)	8.77	9.88	-1.1 ± 5.4	23 ± 8	36 ± 10	7.4 ± 12	1.06
NGC 3900	0.0123 (5,2)	0.0526 (8,7)	5.33	6.36	-0.2 ± 0.3	2.4 ± 1.2	10.5 ± 0.6	1.1 ± 0.7	1.15
NGC 4138	0.0200 (1,3)	0.0448 (6,3)	3.91	5.92	-1.3 ± 0.4	18.4 ± 1.1	18.7 ± 1.2	2.2 ± 1.0	...
NGC 4772	0.0152 (7,3)	0.0809 (5,2)	4.26	4.11	2.4 ± 1.0	19.7 ± 3.5	27.9 ± 3.5	7.8 ± 2.2	1.16
NGC 4866	0.0120 (7,4)	0.1332 (8,6)	3.76	3.50	-0.89 ± 0.4	1.42 ± 0.35	7.0 ± 0.7	0.5 ± 0.8	1.15
NGC 5377	0.0496 (8,6)	0.1584 (8,2)	1.92	4.91	1.65 ± 0.5	4.9 ± 0.8	21.6 ± 2.8	2.4 ± 1.1	1.10
NGC 5448	0.0262 (1,4)	0.0985 (7,6)	1.50	3.00	-1.3 ± 0.8	1.9 ± 0.7	28.4 ± 2.5	1.0 ± 1.7	1.06

that beyond R_{Ho} , the position angle advances in the direction of galactic rotation. Finally, fourth, that gas far beyond R_{Ho} defines a line of nodes differently oriented from that of the inner disk. Here, we comment on the adherence of our sample to these rules of warps.

The characteristic signature in the tip–LON diagram of a galaxy which follows the above rules is a clustering of points representing radii $r < R_{25}$ in the center of the diagram, followed by the outer points spiraling outward to larger tip angles in the direction of galactic rotation. Here, we have typically not been able to determine the direction of rotation, but can see that NGC 1169 clearly shows the signature in the other particulars. The galaxy is roughly planar, though slightly increasing in inclination, to $R_{25} = 125''$. Beyond about $r = 140''$, however, the position angle rapidly and smoothly increases by 25° .

This signature is not as clearly seen in any of the remaining galaxies. NGC 3623 exhibits a gradual inclination decrease over the entire disk, but shows little position angle change. NGC 3626 exhibits steadily changing position angle but steady inclination throughout the truncated disk, well within R_{25} . NGC 3900 exhibits no more than 10° of tip at any radius, except for the first point on the approaching side, which has large errors. NGC 4138 exhibits a spiralling pattern, but one which changes direction abruptly at $\sim 2R_{25}$. NGC 4772 exhibits a spiralling pattern, but there is no apparent transition radius. NGC 4866 shows no warping. NGC 5377 exhibits two regimes: one within $R_{25} = 111''$ in which the position angle smoothly increases, and another beyond R_{25} in which there is no change in i or Γ , but in which these values are different than those of the inner disk. It is also interesting to note that the optical morphological tip angle in NGC 5377, as represented by the starred point in Figure 2, is the only one which does not correspond well with the kinematic tip angles in H I. This discrepancy is due to the presence of separate inner and outer stellar disks, which exhibit very different inclinations and position angles. The H I seems to exhibit tip angles similar to the outer disk, while R_{25} is well within this inner disk. Finally, NGC 5448 exhibits some 20° of position angle change within radii $r \leq .6R_{25}$, but is not warped beyond R_{25} .

The only galaxy in this sample which clearly follows Briggs’ rules, therefore, is the barred SBa galaxy NGC 1169. It is important to note, however, that NGC 1169 is one of only two galaxies in the sample which does not show evidence of peculiar kinematics. The other, NGC 5448, is not warped outside of the inner disk; therefore, we should not expect the rules to apply. Thus, the two kinematically normal galaxies in the sample are consistent with Briggs’ rules for warps. The remaining, kinematically decoupled galaxies, where they exhibit warping, are inconsistent with these rules as a group. While most exhibit warps of some kind, the warps are qualitatively different from the warps observed in kinematically normal galaxies.

4.3. Searching For Trends in Asymmetry

It is important to note for the purposes of this section that the galaxies selected for these observations were mostly gas rich, with H I masses ranging from $10^9 \lesssim M_{HI} \lesssim 6 \times 10^9 M_\odot$, compared to the range of $5 \times 10^8 \lesssim M_{HI} \lesssim 6 \times 10^9 M_\odot$ for Sa galaxies in the Local Supercluster as tabulated by Roberts & Haynes (1994). They also represent a very narrow and red range of colors, with nearly all $B-V$ values near 0.82, compared to ranges of $0.6 \lesssim B-V \lesssim 0.8$ given in Roberts & Haynes as representative of early-type disks. This subset is also small, consisting of only nine objects. Therefore, this sample is not representative of Sa galaxies as a class, and any relationship observed among physical parameters here or any extrapolation to Sa galaxies as a whole should be approached with the utmost caution.

In order to examine the relationships between the kinematic asymmetries observed in the sample and the physical properties of the galaxies, the derived rotation curve asymmetry measure S_2^{drv} presented

in Table 3 was compared to the global optical and H I properties of the sample galaxies presented by Papers I—III. These physical properties were: the $U-B$ color index, the $B-V$ color index, the relative size of the H I disk at a level of $1 M_{\odot} \text{ pc}^{-2}$ to the optical disk R_{HI}/R_{25} , the total blue luminosity $L_B/10^{10} M_{\odot}$, the total H I mass $M_{HI}/10^9 M_{\odot}$, and the H I mass to blue luminosity ratio M_{HI}/L_B . Plots of pairs of these parameters are presented in Figure 3.

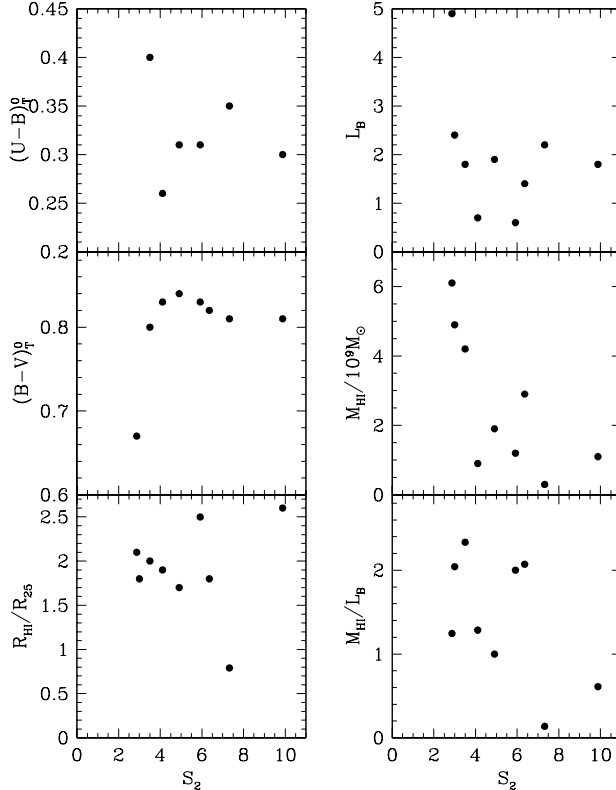


Fig. 3.— Plots of intrinsic physical properties of the Sa sample, as a function of the derived rotation curve asymmetry S_2 . From top to bottom, left to right: the $U-B$ color index, corrected for external and galactic extinction and for redshift from the RC3; the $B-V$ color index, corrected for external and galactic extinction and for redshift from the RC3; the radius at $N_{HI} = 1 M_{\odot} \text{ pc}^{-2}$, R_{HI} , in terms of R_{25} ; total blue luminosity in terms of $10^{10} L_{\odot}$ from Papers I—III; the total H I mass in terms of $10^9 M_{\odot}$ from Papers I—III; and the total H I mass to blue luminosity ratio in terms of M_{\odot}/L_{\odot} .

It appears that galaxies in this sample with smaller H I masses tend to have greater asymmetry measures. That there is no similar trend with R_{HI}/R_{25} indicates that the issue is not a small number of points measured along the rotation curve, whose errors would tend to inflate the measurement of S_2 . It may indicate that smaller galaxies have smaller overall H I masses, making them more susceptible to perturbation. However, the small range of masses probed makes the significance of this tendency uncertain.

The various quantifiers of morphological and dynamical asymmetry derived in Table 3 were also compared to each other, again to search for trends among the various parameters. Figure 4 illustrates the relationships between the morphological asymmetry parameter A_f in the H I to dynamical parameters. No

significant trends are detected between morphological and dynamical parameters. The very weak correlation observed in KHLvZ between A_f and $\langle\Delta\Gamma(\theta)\rangle$ is not recovered.

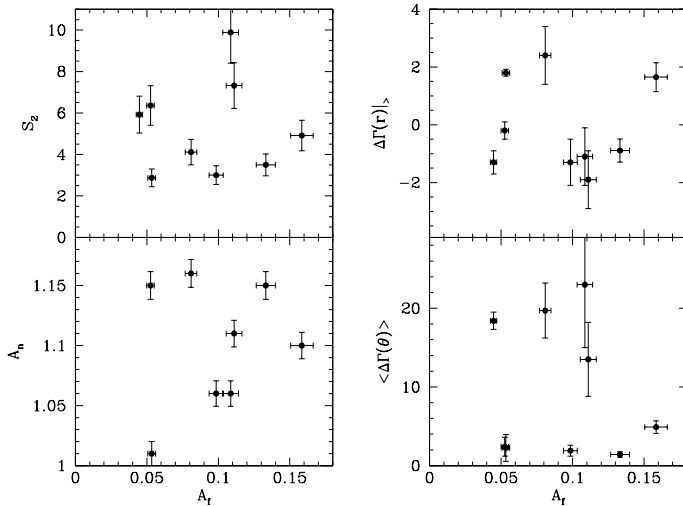


Fig. 4.— Illustration of the relationships between the morphological asymmetry parameter A_f and dynamical asymmetry parameters S_2 , the rotation curve asymmetry, A_n , the line profile asymmetry, $\Delta\Gamma(r)|_>$, the greatest position angle asymmetry in radius, and $\langle\Delta\Gamma(\theta)\rangle$, the average position angle asymmetry between approaching and receding sides.

The physical meaning of this apparent non-correlation is not entirely clear, however. The Sa galaxy sample (Jore 1997) was selected in part based on moderate inclination, which allows the dynamical parameters to be well-constrained, but introduces uncertainty in the determination of the morphological parameters. Furthermore, Sa galaxies are often dusty and show tightly wound spiral structure with patchy star formation regions. Conversely, the face-on aspect of the sample of KHL and KHLvZ constrains the morphological quantifiers, but introduces uncertainty in the dynamical ones.

Figure 5 illustrates the relationships among the dynamical asymmetry parameters. The strongest observed trend is between the derived rotation curve asymmetry S_2^{drv} and the average position angle change between sides, $\langle\Delta\Gamma(\theta)\rangle$, although even this is only marginally detected. This trend could reflect imprecise centering, which would inflate both values together, but such improper centering would also inflate measures of A_f and $\Delta\Gamma(r)$. As no correlation is detected between these values and either S_2 or $\langle\Delta\Gamma(\theta)\rangle$, improper centering can be eliminated as a source of this effect.

This relationship therefore is likely a real physical effect. The simplest explanation of the correlation is that localized streaming motions, which affect the rotation curve and position angle on one side of a galaxy, are detected both in S_2 and $\langle\Delta\Gamma(\theta)\rangle$. More exotic explanations, however, such as mass infall or minor mergers, cannot be ruled out.

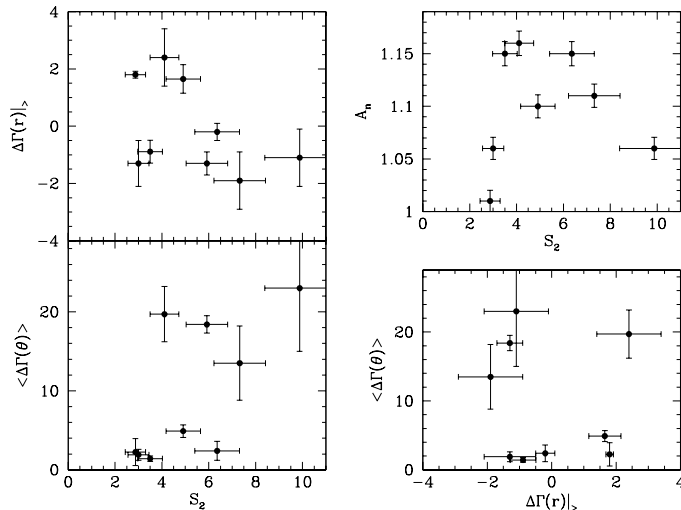


Fig. 5.— Illustration of the relationships among the various dynamical asymmetry parameters, including the derived rotation curve asymmetry S_2^{drv} , A_n , the line profile asymmetry, $\Delta\Gamma(r)|_>$, the greatest position angle asymmetry in radius, and $\langle\Delta\Gamma(\theta)\rangle$, the average position angle asymmetry between approaching and receding sides.

4.4. Comparing S_2 with Global Kinematic Asymmetry

Swaters *et al.* (1999) have found that kinematic lopsidedness as measured by Fourier decomposition was intimately connected with qualitatively asymmetric rotation curves. To test this hypothesis, we apply the method of SFdZ to our sample of nine galaxies to find the zeroth through third harmonic components of each galaxy’s velocity field as a function of radius. In this analysis, only rings with filling factors in excess of 0.5 were considered, to reduce the effects of noise in the outermost rings.

SFdZ define the average amplitude in the i th harmonic component as

$$\sum_j [\hat{c}_i(j)^2 + \hat{s}_i(j)^2]^{1/2} / N, \quad (10)$$

where each of N sampled radii is labeled by j , and the \hat{c}_i and \hat{s}_i are defined by:

$$v_{\text{los}} = v_{\text{sys}} + \sum_n \hat{c}_n \cos n\hat{\psi} + \hat{s}_n \sin n\hat{\psi}, \quad (11)$$

where $\hat{\psi}$ is the azimuthal angle from the major axis in the plane of the galaxy. The exception is the $i = 1$ harmonic, in which $\hat{c}_1(r)$ is V_{rot} , and the first harmonic component is taken to be the average of the \hat{s}_1 terms. The error analysis conducted here follows the discussion of SFdZ, but it is important to note that the error bars presented in the following figures represent only the formal numerical error. Systemic errors due to random velocities in gas clumps may also be of similar order.

These results were then plotted against our measure of rotation curve asymmetry S_2^{drv} . The results are presented in Figure 6, in which each frame traces a harmonic component as a function of S_2 in the sample. In agreement with Swaters *et al.* (1999), we find that the rotation curve asymmetry measure S_2 is correlated with the $n = 2$ Fourier mode. Trends of increasing $n = 1$ and $n = 3$ are also observed

for increasing S_2 . In addition, S_2 values for the rotation curves of the kinematically asymmetric galaxies DDO 9 and NGC 4395 studied by Swaters *et al.* would also clearly be large. We therefore conclude that S_2 is a good first indicator of asymmetry in disk kinematics as measured by Fourier decomposition.

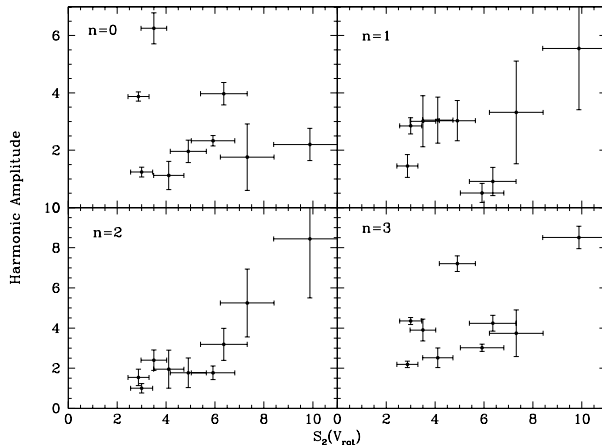


Fig. 6.— Illustration of the relationships between the derived rotation curve asymmetry parameter S_2^{drv} and the $n = 0, 1, 2, 3$ dynamical harmonic components as measured by the method of SFdZ.

4.5. Conclusions

We have examined the morphological and dynamical H I symmetry properties of a sample of moderately inclined, morphologically normal Sa galaxies. These galaxies were known previously to exhibit kinematic peculiarities ranging from warps to extended counter-rotating disks, and are possibly the remnants of minor mergers.

This work confirms the normal optical morphology for which this sample was selected, and finds significant deviations from symmetry in both H I morphology and dynamics. This result reinforces earlier findings that normal morphology is not an indicator of normal kinematics, and conversely, that perturbed kinematics do not necessarily manifest as perturbed optical morphology. Thus it appears that the time required for the optical (stellar) component to recover from the perturbative events which generated the distinct kinematics is smaller than the time required for the gas to recover.

We have analyzed the circumstances of warping in the H I disks following the discussion of Briggs (1990), in which it is found that simple warps exhibit a common structure of changing inclination within the optical radius, followed by advancing position angle in the direction of rotation outside of the optical radius. We find that warps in the kinematically peculiar galaxies exhibit more complex behavior than do the common warps seen in Briggs’ sample.

The warping observed in the majority of the Sa galaxies is of the 15° order in “tip” angle, as predicted by the numerical simulations of minor mergers illustrated by Quinn *et al.* (1993) and Hernquist & Mihos (1995). The weak trend found in this sample between global $n = 1$ and $n = 3$ asymmetry and rotation curve asymmetry S_2 , measuring non-circular motions, is also consistent with the excitation of these modes

due to minor mergers predicted by Hernquist & Mihos. Those authors also predict the formation of a highly non-axisymmetric potential in the final stages of the merger, as well as morphological “clumping” of the gas as opposed to the smoother distribution of stars. Such predictions are consistent with the high values of S_2 and $\Delta\Gamma$ measured in this sample, as well as the striking differences in optical versus gas morphologies.

We have also demonstrated the effectiveness of a simple rotation curve asymmetry measure, specifically S_2 , for identifying galaxies with global kinematic asymmetry. This quantifier, in conjunction with the position angle and line profile measures, are methods by which dynamical asymmetry may be estimated quickly and thus suggest a way to search large catalogs of rotation curves for galaxies which exhibit lopsidedness or decoupling.

Further work will be required to determine whether these findings are represented by the larger class of Sa galaxies. It will also be important to consider direct comparisons between the velocity fields of numerical simulations and observed velocity fields and their asymmetry measures, for it is in the dynamics that minor merger remnants are identified.

This work has been partially supported by NSF grants AST-9528860 and AST-9900695 to MPH, and by National Space Grant College and Fellowship Program grant NGT-40019 to DAK. This research has made use of the NASA/IPAC Extragalactic Database (NED) which is operated by the Jet Propulsion Laboratory, California Institute of Technology, under contract with the National Aeronautics and Space Administration.

REFERENCES

- Begeman, K. G. 1989. *A&A*, 223, 47.
- Bertola, F., Cinzano, P., Corsini, E. M., Pizzella, A., Persic, M., & Salucci, P. 1996, *ApJ*, 458, L67
- Briggs, F. H. 1990, *ApJ*, 352, 15
- Buta, R., van Driel, W., Braine, J., Combes, F., Wakamatsu, K., Sofue, Y., & Tomita, A. 1995. *ApJ*, 450, 593
- Ciri, R., Bettoni, D., & Galletta, G. 1995, *Nature*, 375, 661
- Conselice, C.J. 1997, *PASP*, 109, 1251.
- Corsini, E. M., Pizzella, A., Funes S. J., J. G., Vega Beltrán, J. C., & Bertola, F. 1998, *A&A*, 337, 80
- de Vaucouleurs, G., de Vaucouleurs, A., Corwin, H.G., Buta, R.J., Paturel, G., & Fouqué, P., 1991. *Third Reference Catalogue of Bright Galaxies* (RC3), University of Texas Press, Austin
- GISPY, The Groningen Image Processing System*. 2000, <http://thales.astro.rug.nl/~gipsy/>
- Haynes, M. P., Giovanelli, R., & Roberts, M. S. 1979, *ApJ*, 229, 83
- Haynes, M. P., Hogg, D. E., Maddalena, R. J., Roberts, M. S., & van Zee, L. 1998, *AJ*, 115, 62
- Haynes, M. P., Jore, K. P., Barrett, E. A., Broeils, A. H., & Murray, B. M. 2000, *AJ*, 120, 703 (Paper II)
- Hernquist, L. & Mihos, C. 1995, *ApJ*, 448, 41
- Jore, K. P., Broeils, A. H., & Haynes, M. P. 1996, *AJ*, 112, 438 (Paper I)
- Jore, K. P. 1997, Ph. D. thesis, Cornell University
- Jore, K. P., Haynes, M. P., Barrett, E. A., & Broeils, A. H. 2000, in preparation (Paper III)
- Kornreich, D. A., Haynes, M. P., & Lovelace, R. V. E. 1998, *AJ*, 116, 2154 (KHL)
- Kornreich, D. A., Haynes, M. P., Lovelace, R. V. E., & van Zee, L. 2000, *AJ*, 120, 139 (KHLvZ)
- Merrifield, M. R., & Kuijken, K. 1994, *ApJ*, 432, 575
- Quinn, P. J., Hernquist, L., & Fullagar, D. P. 1993, *ApJ*, 403, 74
- Roberts, M. S., & Haynes, M. P. 1994, *ARA&A*, 32, 115
- Sandage, A. & Tammann, G.A. 1987, *Revised Shapley Ames Catalogue of Bright Galaxies*, Carnegie Inst. of Washington Publ. 635
- Schoenmakers, R. H. M., Franx, M., de Zeeuw, P. T. 1997, *MNRAS*, 292, 349 (SFdZ)
- Swaters, R.A., Schoenmakers, R. H. M., Sancisi, R., & van Albada, T. S. 1999, *MNRAS*, 304, 330
- Thakar, A. R., Ryden, B. S., Jore, K. P., & Broeils, A. H. 1997, *ApJ*, 479, 702
- van der Hulst, J. M., Terlouw, J. P., Begeman, K., Zwitter, W., & Roelfsema, P. R. 1992, in *Astronomical Data Analysis and Systems*, edited by D. Worall, C. Biemesderfer, & J. Barnes, ASP Conf. Series no. 25, 131
- Zaritsky, D., & Rix, H.-W. 1997, *ApJ*, 477, 118